

Microfluidic device to study arterial shear-mediated platelet-surface interactions in whole blood: reduced sample volumes and well-characterised protein surfaces

Nigel J. Kent · Lourdes Basabe-Desmonts ·
Gerardene Meade · Brian D. MacCraith ·
Brian G. Corcoran · Dermot Kenny · Antonio J. Ricco

Published online: 23 July 2010
© Springer Science+Business Media, LLC 2010

Abstract We report a novel device to analyze cell-surface interactions under controlled fluid-shear conditions on well-characterised protein surfaces. Its performance is demonstrated by studying platelets interacting with immobilised von Willebrand Factor at arterial vascular shear rates using just 200 μL of whole human blood per assay. The device's parallel-plate flow chamber, with 0.1 mm^2 cross sectional area and height-to-width ratio of 1:40, provides uniform, well-defined shear rates along the chip surface with negligible vertical wall effects on the fluid flow profile while minimizing sample volumetric flow. A coating process was demonstrated by

ellipsometry, atomic force microscopy, and fluorescent immunostaining to provide reproducible, homogeneous, uniform protein layers over the 0.7 cm^2 cell-surface interaction area. Customized image processing quantifies dynamic cellular surface coverage vs. time throughout the whole-blood-flow assay for a given drug treatment or disease state. This device can track the dose response of anti-platelet drugs, is suitable for point-of-care diagnostics, and is designed for adaptation to mass manufacture.

Keywords Shear activation · Microfluidics · Platelet-surface interactions · Protein characterisation · Image analysis

Electronic supplementary material The online version of this article (doi:10.1007/s10544-010-9453-y) contains supplementary material, which is available to authorized users.

N. J. Kent · L. Basabe-Desmonts · B. D. MacCraith ·
A. J. Ricco (✉)
Biomedical Diagnostics Institute, Dublin City University,
Glasnevin Dublin 9, Ireland
e-mail: ajricco@stanford.edu

G. Meade · D. Kenny
Biomedical Diagnostics Institute, Dept of Molecular and Cellular
Therapeutics, Royal College of Surgeons in Ireland,
123 St Stephens Green,
Dublin 2, Ireland

B. G. Corcoran
School of Mechanical and Manufacturing Engineering,
Dublin City University,
Glasnevin Dublin 9, Ireland

N. J. Kent (✉)
The Biomedical Devices and Assistive Technology Research
Group, College of Engineering and Built Environment,
Dublin Institute of Technology,
Bolton St.,
Dublin 1, Ireland
e-mail: nigel.kent@dit.ie

1 Introduction

Advances in microfluidic technology are driving the development of new analytical protocols by shrinking sample and reagent volumes, shortening analysis times, reducing transfers and other manual steps, improving accuracy, and enabling parallel analyses (Daw and Finkelstein 2006; Garcia-Cordero and Ricco 2008). Small dimensions and integration of disparate process functions, together with the promise of compact integrated analysis systems and lower cost per test, suit these platforms to everything from high-throughput analysis to point-of-care (POC) testing (Daw and Finkelstein 2006; Ahn et al. 2004; Becker and Locascio 2002; Yager et al. 2008).

In addition to the functional features offered by microfluidic devices, such applications as POC testing typically require low-cost device mass manufacture, for which modern plastic fabrication processes can be effective. To bridge the gap between research and manufacture, several plastic fabrication techniques now enable construction of

prototype microfluidic devices by researchers who are not specialists in fabrication (Whitesides et al. 2001; Boone et al. 2002), leading to increasingly widespread development of application-focused microfluidic devices by researchers in the biomedical and diagnostics fields.

In an application area important to biomedical research and POC diagnostics alike, microfluidic platforms enable the study of single cells and cell populations by effectively handling small fluid volumes, accurately controlling fluid dynamics (e.g., shear), localizing compound delivery, providing local analysis of small numbers of molecules, and facilitating the imaging of cellular morphological changes *in situ* and in real time (El-Ali et al. 2006). A particularly promising application of microfluidically enabled cellular analysis is the study of shear-force-dependent interactions between cells and protein surfaces at physiologically relevant shear levels (Thomas 2008). For example, vascular endothelial cells undergo significant morphological changes in response to fluid shear forces, and certain cells or cell fragments, such as leukocytes and platelets, translocate (“roll”) along blood vessel walls, in effect patrolling for points of inflammation or injury at which to react in a manner often modulated by local fluid shear conditions.

Real-time monitoring of the responses of cells interacting with protein surfaces can elucidate the behaviour of a cell or a population of cells, characterising abnormal behaviour and providing the basis for a diagnostic tool. Despite much study, however, the physical and biochemical mechanisms of shear-mediated cell-surface interactions are not yet fully understood, and to date have been studied only sparsely using microfluidic platforms (Chang et al. 2005; Gutierrez et al. 2008; Lu et al. 2004; Fillafer et al. 2009; Schmidt et al. 2008; Saeidi et al. 2009; Schaff et al. 2007).

Two critical enablers for such cell-surface studies and eventual diagnostic tools using microfluidics are (1) the production of reliable fluidic platforms to provide appropriate measurement conditions and environments, and (2) the in-depth understanding and control of the morphology, structure, and function of active protein surfaces, coupled with a reproducible means of deposition on the fluidic platform. Device substrate material, protein delivery method, and immobilisation technique all can impact the final density, conformation, and functionality of a surface-confined protein layer (Nakanishi et al. 2001). In defining and characterizing the protein surface, parameters of interest include the thickness and density of the protein, its conformational changes upon surface attachment, and functionality of (inter) active protein components post surface attachment.

Because activating surface proteins are central to human platelet function in whole blood, they offer a relevant, attractive application target for study of shear-mediated cell-surface interactions (Kroll et al. 1996; Harrison 2005). Platelets or thrombocytes—small, discoid ($2\text{--}4 \times 0.5 \mu\text{m}$)

cell fragments that circulate in the bloodstream—are involved in the cellular mechanisms of hemostasis that lead to the formation of blood clots. Under normal vascular conditions, the endothelium provides a non-thrombotic surface, promoting efficient blood flow. If, however, the endothelium is altered or a vessel wall damaged, a combination of extracellular proteins is exposed, regulating a complex functional response in platelets and resulting in the rapid formation of a “plug” that occludes the site of injury to prevent blood loss. The initial stages of these interactions are dominated by the exposure of von Willebrand Factor (VWF), an activating protein uncovered by vascular damage. These VWF-platelet interactions are highly shear force dependent (Michelson 2006).

While the choice of research test method presently depends on the particular aspect of platelet function under investigation, the standard tool to study shear-mediated responses in platelets under defined flow conditions is a parallel-plate flow chamber (Kantak et al. 2003). The defining characteristic of this device is the low aspect ratio of the sample flow path, resulting in an almost-constant wall shear force over an area of the device suitable for protein deposition and imaging of significant numbers of platelets in a microscope’s field of view. While many research groups have designed and constructed custom flow chambers (Gutierrez et al. 2008; Kantak et al. 2003; Mody et al. 2005), the parallel-plate devices commercially available from Glycotech are widely used (Brown and Larson 2001). Assembly of multiple parts is required to form a complete Glycotech chamber; a vacuum pump is needed to seal together the various chamber components.

For clinical hemodynamic studies, the assembly of the flow chambers and subsequent sample introduction are technically laborious, requiring training and experience. In addition, the volume of blood sample required for a single hemodynamic experiment can be considerable (just under 5 mL of whole blood for a 120-sec run). Nonetheless, an attractive characteristic of these systems is the possibility of generating significant amounts of data from a single experiment with a single sample. The data typically take the form of fluorescent image sequences obtained at user-defined intervals during a “flow run”. At appropriate magnifications, these images can contain both single-platelet-specific data and information pertaining to the entire platelet population of the donor or patient.

To date, analysis of data from parallel-plate flow chambers has proved challenging: while image-based platelet function analysis has been reported, it typically involves significant sample manipulation, including sample (blood or plasma) dilutions or laborious manual image analysis, and ultimately uses only a fraction of the captured data. An increasing need for flow-based assays to evaluate thrombosis, hemostasis, and bleeding risk under fluid shear conditions has been recognized (Zwaginga et al. 2006a, b). Highlighting challenges with

current analytical approaches, a recent official communication by the scientific and standardization committee of the International Society on Thrombosis and Hemostasis (ISTH) made recommendations (Zwaginga et al. 2007) for use and development of flow tests, including:

1. Use of controlled (quantity of) collagen as adhesive substrate
2. Use of multiple shear rates
3. Use of non-anticoagulated blood, preferably at physiological cation concentrations
4. Use of single-pass, small-capacity (volume) flow devices
5. Time-dependent measurement of thrombus build-up.

In this paper, we report design, construction, and characterization of a microfluidic device for the characterisation and study of platelet-surface interactions on well-defined protein surfaces. We also report a method for reproducible deposition and characterisation of the protein surfaces, in particular VWF, that are a key component of successful platelet/protein interaction assays. The device requires significantly less blood—approximately 30-fold less volume for the same flow time—than current commercial parallel-plate devices, making it useful for mouse experiments or neonatal blood analysis. We further report our development of custom software to measure surface coverage of adhered platelets from blood samples, validating the overall assay device concept and highlighting its potential as a useful diagnostic tool.

2 Experimental methods and materials

2.1 Device development

2.1.1 Parallel plate flow theory

The flow of a fluid with viscosity μ between two fixed, infinitely wide parallel plates of length L , separated by distance a is shown in Fig. 1.

This configuration can be assessed by assuming a time-invariant pressure drop in the direction of L (defined here as

the x direction), in which case the Navier-Stokes relationship between the gradient of fluid velocity, u , in the z direction and the positional rate of change (slope) of the pressure, p , in the x direction can be simplified to yield

$$\frac{\partial^2 u}{\partial z^2} = \frac{1}{\mu} \frac{dp}{dx}. \quad (1)$$

Solving Eq. 1 and assuming a channel width b in the y direction, the volumetric flow rate Q can be approximated by:

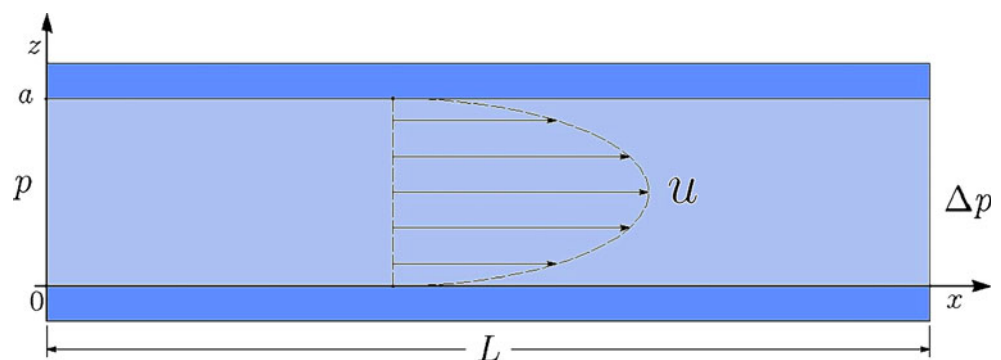
$$Q = \int_0^b dy \int_0^a \frac{1}{2\mu} \frac{dp}{dx} (z-a)z dz = \frac{a^3 b}{12\mu} \frac{dp}{dx}. \quad (2)$$

Since Eq. 1 is based on the assumption of infinitely wide parallel plates, it follows that the approximation of flow rate calculated by Eq. 2 is highly aspect-ratio dependent and breaks down as the aspect ratio approaches one. In the case of an aspect ratio of one third, ($a=b/3$), the error is as much as 23%, falling to 7% for an aspect ratio of one tenth, ($a=b/10$) (Bruus 2007).

Despite these limitations, Eq. 2 is typically used to develop the shear force equations through parallel-plate flow devices because typical aspect ratios are on the order of one twentieth to one fiftieth. The main reason for utilizing such low-aspect-ratio chambers is evident if the velocity profiles for two-dimensional flow through a rectangular duct are plotted over a range of aspect ratios as shown in Fig. 2.

As the aspect ratio decreases, the impact of the vertical wall on the overall velocity profile decreases and the flow can be assumed to be one dimensional, as in Eq. 2. This results in a constant velocity profile across nearly the entire chamber width, (Fig. 2, aspect ratio 1:40) resulting in shear force being imparted on the particles (e.g., platelets) in primarily one direction, facilitating the control of important experimental parameters and simplifying analysis. While particles close to the vertical wall will undergo shear forces in two directions, appropriate flow path dimensions can be chosen to ensure only those particles subject to one-dimensional shear forces are within the field of view.

Fig. 1 Schematic diagram showing pressure-driven flow in the $+x$ direction between infinitely wide (in the $\pm y$ direction, perpendicular to the page) parallel plates, where a is the spacing between plates in the z direction, L is the length of the plates along x , p is the pressure at $x=0$, Δp is the pressure difference (drop) between $x=0$ and $x=L$, and u is the fluid velocity in the x direction



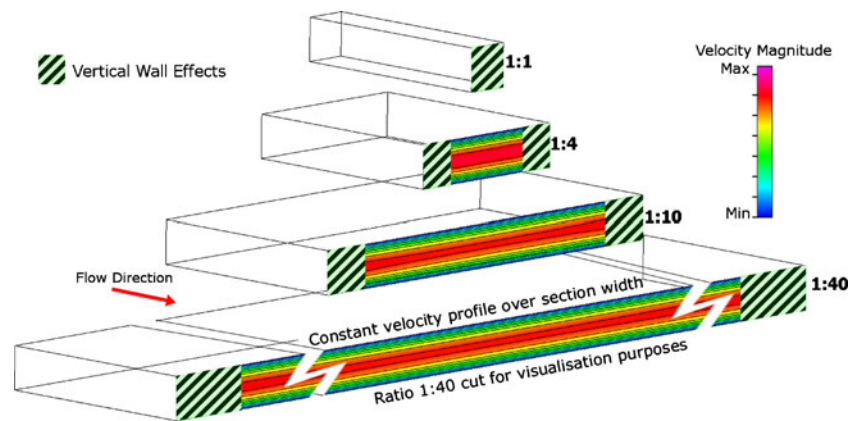


Fig. 2 Depiction of effect of channel aspect ratio on flow profile. At an aspect ratio (height:width) of 1:1, the vertical and horizontal walls of the device contribute equally to the flow profile. As this aspect ratio decreases, the effect of the vertical walls (hatched overlay indicates

where the profile differs by at least 1% from that at the center of the channel) becomes less relevant to the overall flow profile, and the flow can be considered one dimensional. The aspect ratio for the device reported in this article is 1:40

The wall shear force (also known as shear stress), τ_w , can be calculated in terms of chamber dimensions, fluid viscosity, and volumetric flow rate using

$$\tau_w = \frac{6\mu Q}{a^2 b} \quad (3)$$

2.1.2 Device fabrication

The hybrid multilayer parallel-plate flow device, designed to simplify the assembly process, is suitable for adaptation to low-cost mass manufacture. It consists of a polymethylmethacrylate (PMMA) top plate with inlet and outlet connections, a pressure-sensitive adhesive (PSA) flow-path-defining layer, and a glass coverslip base plate (Fig. 3).

For the top plates, 6-mm-thick PMMA stock (Ensinger Plastics, UK) was machined to standard microscope slide dimensions, 75 mm long \times 25 mm wide, using conventional milling. This piece was then drilled and tapped to accept inlet and outlet connection ports (the top plates would be made by injection molding for mass manufacture). The middle layer material, which defines the flow path, is a commercially available double-sided PSA laminate: ARCARE[®]8890 (Adhesives Research, Limerick Ireland) is a 12.5- μ m polyester film coated on both sides with medical-grade acrylic adhesive, resulting in an overall thickness of 50 μ m. The flow path layer was cut using a Coherent GEM-100[™] liquid-cooled CO₂ laser embedded in a Micro-master Turnkey dual-head laser system from Optec SA, Belgium.

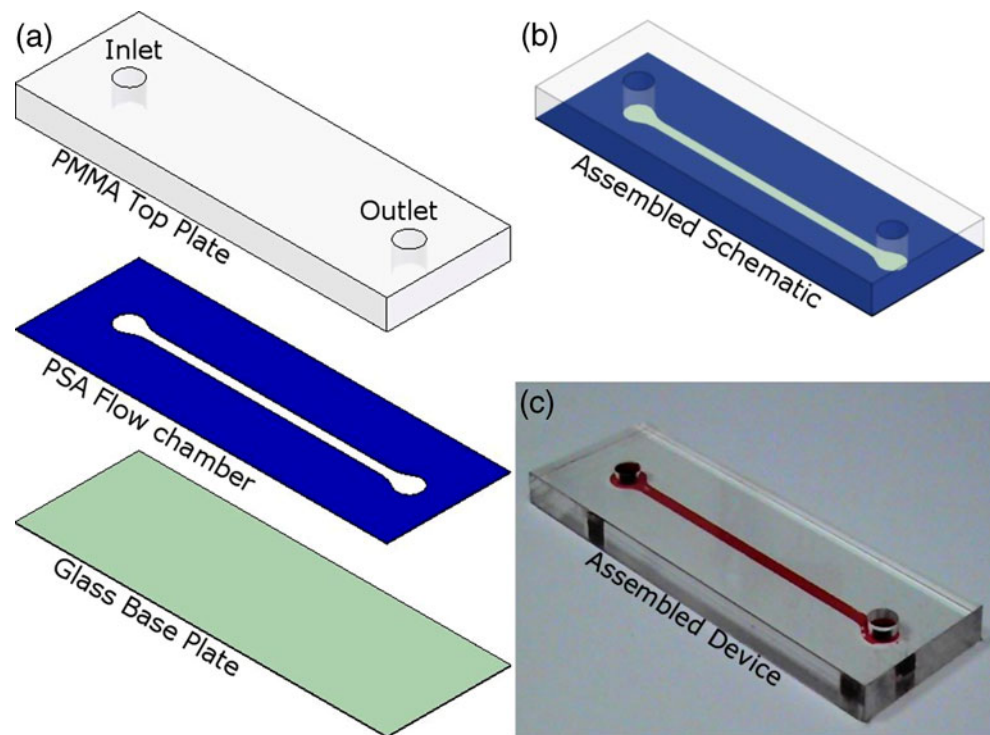
As with the top plate, the outer dimensions of the PSA laminate layer correspond to microscope slide dimensions. Flow chamber height is determined by the laminate height, 50 μ m, while the flow width is laser patterned to 2 mm, resulting in an aspect ratio of 0.025 (1:40) and a cross

sectional area of 0.1 mm², compared to a cross sectional area of 1.27 mm² for the Glycotech commercial flow chambers. In practical terms, this results in a 97% reduction of the volumetric flow rate required to generate an arterial shear rate of 6 N/m², from 2.4 mL/min to 75 μ L/min. As the flow path is a critical aspect of the design, this fabricated layer was characterised with using white-light interferometry techniques (see Results section) using a WYKO NT100 from Veeco.

The base layer of the platform is a commercially available glass microscope coverslip, chosen for three reasons: (1) the majority of standard protein deposition and characterisation techniques are well established on glass surfaces; (2) the thickness and refractive index of the slides are compatible with existing oil-immersion lenses for optical detection of platelet surface interactions at appropriate lateral and depth resolution; (3) high quality glass coverslips are a widely available commodity with tightly controlled dimensional, optical, and surface-finish tolerances, in addition to having predictable, reliable surface chemistry. Both glass coverslip and machined top plate are washed with absolute ethanol which is then allowed to evaporate prior to chamber assembly, then rinsed by perfusion with phosphate-buffered saline (PBS) post assembly.

To assemble the device, the glass coverslip is placed in a custom-machined alignment jig and one release liner is removed from the PSA layer, which is then aligned with and adhered to the glass coverslip. The remaining release liner is then removed from the PSA layer and the PMMA top plate is aligned with and adhered to the exposed PSA surface. The entire assembly is then removed from the jig and pressed together through two rollers to form the sealed device. The inlet and outlet fittings are 1/16-in threaded polypropylene connectors for connection to 1/16-in inner diameter silastic[™] tubing, both available from Glycotech.

Fig. 3 Parallel-plate blood-flow device schematic. (a) Exploded view of the constituent components of the device: PMMA top plate, laser-patterned PSA layer, and the glass (microscope coverslip) base plate. (b) The layers of part (a) shown fully assembled. (c) Photograph of an assembled, fully functional device (dye added for visualisation purposes)



2.2 Protein layer deposition

2.2.1 Substrate preparation for ellipsometry and atomic force microscopy (AFM)

Oxide-coated silicon wafers (Universitywafer.com, Boston, MA) were used as substrates for protein layer deposition and subsequent characterisation using both AFM and ellipsometric techniques. The thickness of the native oxide layer on the silicon wafers lies between 0.3 and 1 nm. Due to the high refractive index of silicon relative to the biological layers being characterised, ellipsometric measurements on this substrate are far more precise than on glass (Tengvall et al. 1998a; Toscano and Santore 2006).

Oxidized silicon wafers and glass have very similar surface chemical composition (predominantly SiO₂) and reactivity properties, so Si wafers are often used as surrogates for glass surfaces. Four-inch polished, <100>-oriented, P-doped (n-type) silicon wafers were cut into approximately 2×2 cm samples. All substrates were rinsed with MilliQ water and dried with N₂ before use.

2.2.2 Adsorption of VWF protein for surface studies

Aqueous solutions of VWF (a gift of Prof. Robert Montgomery, Blood Research Institute, Milwaukee, USA) in PBS (0.01 M phosphate buffer, 0.0027 M potassium chloride, 0.137 M sodium chloride, pH 7.4; Sigma Aldrich, Ireland) at concentrations ranging from 1 to 1,000 µg/mL were prepared. Before adsorption onto glass or SiO₂

surfaces, the protein solutions were maintained at 37°C in a water bath. 100 µL of VWF solution were placed on the center of the sample substrate and allowed to adsorb for 2 hr. To avoid evaporation, the samples were placed in a simple environmental chamber, a plastic petri dish containing a few millilitres of water. The sample was supported in the petri dish such that contact between the sample and the water was avoided. Each sample was subsequently rinsed with 2 mL of PBS followed by rinsing with a stream of MilliQ water for approx. 10 s to remove any PBS salts remaining on the surface. The samples were then dried with a stream of N₂ for a period of 5 to 10 s and the ellipsometric thickness was measured and/or AFM images obtained. All VWF surfaces were prepared and measured at least twice.

2.2.3 Surface preparation and VWF deposition for flow chambers

After assembly, the flow chamber was filled with a 100 µg/mL VWF solution in PBS and incubated for 2 h at room temperature to coat the inner bottom surface with the protein.¹ The VWF-coated coverslip was then "blocked"

¹ Some protein is expected to adsorb onto the PMMA surface; however, this should not affect the results, as the depth of focus, which is centered on the fluid-contacting surface of the glass bottom plate, is only 20 µm (objective working distance=190 µm, slide thickness=170 µm); furthermore, the flow conditions are such that any platelet that interacts with a side wall or the top plate will not reach the bottom plate within the microscope's field of view.

against adsorption onto any remaining “active” (adsorption-prone) surface regions by static incubation with 1% BSA (Sigma Aldrich, Ireland) in PBS for 1 hr, and finally washed by gentle perfusion with at least 3 mL of PBS prior to introducing blood sample. The chambers were typically prepared on the morning of the experiments and stored at room temperature prior to use.

2.3 Protein layer characterisation

2.3.1 Ellipsometry

Layer thicknesses were evaluated with a DeltaPsi2 Spectroscopic Ellipsometer at $\lambda=630, 635, \text{ and } 640 \text{ nm}$, with incident angle of 75° . To calculate the ellipsometric thickness of the VWF layer, a two-layer model— SiO_2 and VWF being the layers—was used. A refractive index of 1.465 was assumed for the VWF layer (Elwing 1998; Tengvall et al. 1998b). The spot size of the incident light on the substrate was $5 \times 1.5 \text{ mm}^2$.

2.3.2 AFM

AFM studies were performed with a commercial instrument (Dimension 3100 AFM with Nanoscope IIIa controller equipped with a phase-imaging extender, Digital Instruments) operating in tapping-mode (TM-AFM), using standard silicon tips (Tap300Al, BudgetSensors, Bulgaria) with 42 N/m nominal spring constant and 300 kHz nominal resonant frequency. All images were recorded in air at room temperature, at a scan speed of 1–1.5 Hz. The background slope was resolved using first- or second-order polynomial functions. No further filtering was performed.

2.3.3 Fluorescent assay of VWF layer uniformity

Glass coverslips (75 mm \times 25 mm coverslips, Bio-World Ltd, Dublin, OH, USA) were incubated with varying concentrations of VWF (300 μL of 1 to 100 $\mu\text{g}/\text{mL}$ VWF in PBS) for 2 h at room temperature and washed with PBS buffer (minimum of 3 washes). Coverslips were stained with sheep-anti-human fluorescein isothiocyanate (FITC)-labeled anti-VWF antibody (1/100 dilution; AbD Serotec, UK) for 1 h at room temperature, washed with PBS and mounted with DAKO fluorescence mounting medium (Dako Diagnostics, Ireland). A sheep-anti-human FITC-labeled negative control antibody (AbD Serotec, UK) was used to control for any non-specific staining (data not shown). Slides were viewed with a Zeiss LSM-510 META Axioplan-2 laser scanning microscope (Carl Zeiss, Jena, Germany), using a 63 \times Plan-Apochromat oil immersion objective (NA: 1.4) with the same scanning parameters (excitation laser 488 nm at 2.1%, emission band-pass filters

505–550, scan zoom 4, detector gain 620). Data were analysed using LSM-510 version 3.2 software.

2.4 Whole blood assays

2.4.1 Blood preparation and platelet labeling

To characterize the performance and diagnostic potential of the parallel-plate blood-flow device, minimally treated whole human blood was compared to whole blood to which the c7E3-Fab fragment ReoPro was added. ReoPro inhibits the $\alpha\text{IIb}\beta_3$ receptor on the platelet surface, thus inhibiting stable adhesion to the VWF surface (Tam et al. 1998), making it a suitable test case for performance characterization of the device.

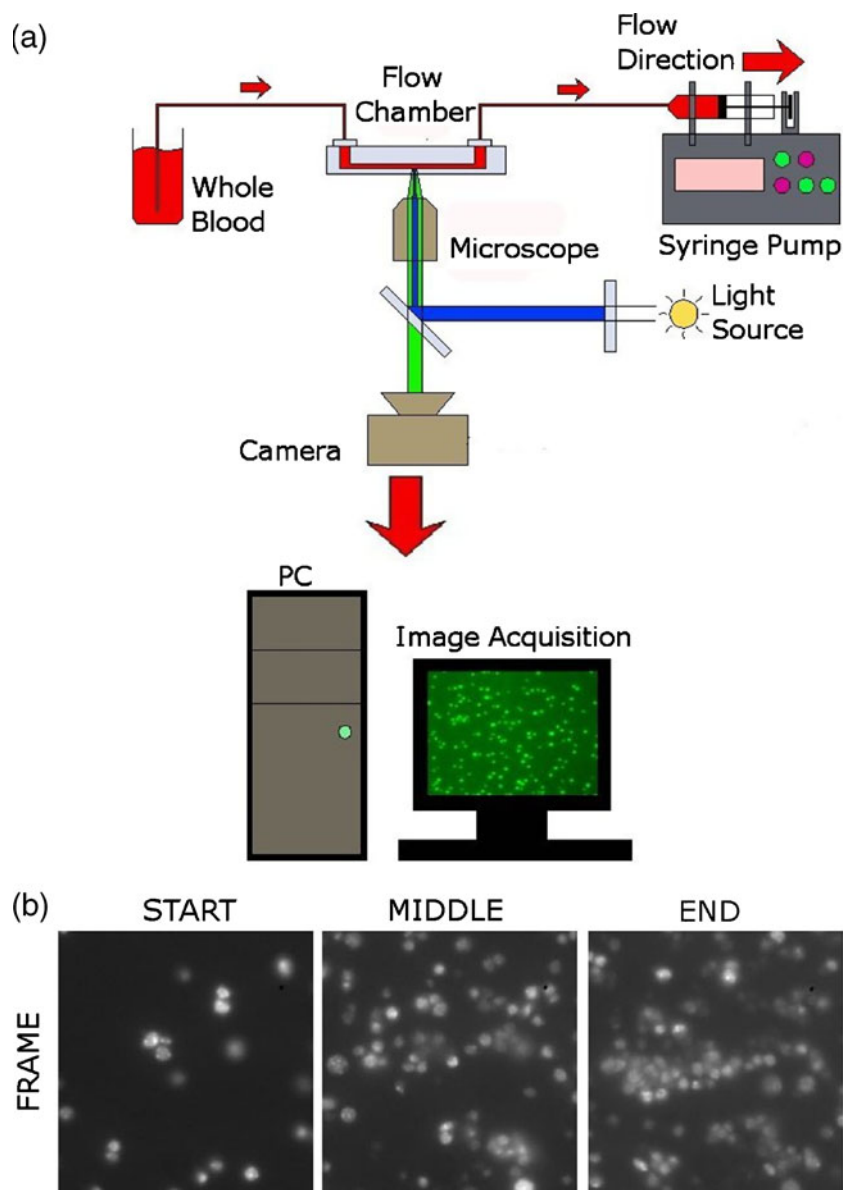
Whole blood was drawn from the antecubital vein of healthy donors, who were not known to have taken any medication within the previous 10 days, using a 19-gauge needle. The first 5 mL of drawn blood was routinely discarded to prevent any possible activation of platelets, and blood was collected in a clean polypropylene syringe containing trisodium citrate as anticoagulant (final concentration of 0.32%, 1:9 ratio of citrate to blood). In the case of ReoPro-treated whole blood, ReoPro (20 $\mu\text{g}/\text{mL}$ final concentration in blood; Eli Lilly & Co., Indianapolis, USA) was added to the whole blood sample 20 min prior to experimental analysis. For fluorescence imaging of platelets, whole blood was labelled with DiOC6(3) (1 μM ; Invitrogen USA), a fluorescent dye commonly used for platelet function studies, by addition and gentle mixing by inversion followed by incubation for 10 min prior to experimental analysis at 37°C .

2.4.2 Measurement system and protocol

Figure 4(a) is a schematic of the experimental system, including a Harvard PhD 2000 syringe pump from Harvard Apparatus to generate the required volumetric flow rate through the device and a Zeiss Axiovert-200 epi-fluorescence microscope (Carl Zeiss Light Microscopy, Germany) to image platelet-surface interactions using a liquid-cooled Quantix-57 CCD camera (Photometrics Ltd, Tuscon, AZ, USA) that records adhesion events and saves them to a PC for subsequent analysis. Figure 4(b) shows typical captured images from the start, middle, and end of a standard flow run; the field of view is $267 \times 256 \mu\text{m}$. The images are captured downstream of any flow-chamber entrance effects and in a central location across the width of the 2-mm-wide channel to ensure vertical wall effects are negligible.

Whole blood samples were assayed at a wall shear force (stress) of $6 \text{ N}/\text{m}^2$, which, assuming constant blood viscosity of $0.004 \text{ Pa}\cdot\text{s}$ (4 cP), occurs at a volumetric flow

Fig. 4 (a) Experimental setup for detection of shear-mediated platelet–surface interactions. (b) Images at the start, middle, and towards the end of a 125-sec whole blood flow analysis sequence, showing qualitatively how the surface platelet coverage evolves over the course of the run



rate through the device of $75 \mu\text{L}/\text{min}$ and corresponds to an arterial wall shear rate of $1,500 \text{ s}^{-1}$ (in the arterial range (Kroll et al. 1996)). In all cases, whole blood samples were assayed within 2 h of the initial blood draw. For each experiment, 3,000 images were recorded at a capture rate of 24 frames/s, corresponding to an overall run time of 125 s; in that time, a total blood volume of $156 \mu\text{L}$ was consumed. In comparison to the existing commercial system, wherein 5 mL would have been consumed under the same shear force conditions for the same analysis time, this represents a significant reduction in sample volume required. We note here that recent measurements in our laboratories show that as few as 21 s of images at the start of such a run can be sufficient to reveal significant differences in platelet populational characteristics (Lincoln et al. 2010), suggesting that a blood volume of $<100 \mu\text{L}$ would be adequate for

some measurements based on this technology, permitting, for example, its use for mouse studies and assays on neonatal blood samples.

2.4.3 Image analysis software

Acquired images pass through a custom-designed algorithm to determine surface coverage of adhered platelets. In the first step, individual objects (platelets) within each image (frame) are detected using custom software developed in the LabVIEW environment (National Instruments, TX, USA). Object detection is based primarily on fluorescent intensities of platelets relative to background. To increase throughput and eliminate operator bias, an automated algorithm assigns those pixels with a value above a predetermined threshold a numeric value of one and those

below the threshold a value of zero. This threshold limit is automatically calculated on a frame-by-frame basis using the ‘Metric’ thresholding option included in the LabVIEW image processing development suite (NI Vision Concepts Manual 2000).

A frame-by-frame calculation of threshold limit allows the threshold value to be optimised over a single flow run. This feature is particularly useful towards the end of a series of images, where increased numbers of platelets in the field of view may contribute significantly to the background noise of the image, making a static threshold limit difficult to implement robustly. To determine surface coverage for each frame, the software calculates the total area covered by pixels having a value of one as a percentage of the total number of pixels in the overall frame area.

3 Results and discussion

In accord with the recommendations of the ISTH (Zwaginga et al. 2007), minimally treated whole human blood was selected as the sample, eliminating the lengthy preparation process often required for shear-mediated platelet studies using platelet-rich plasma while diminishing the possibility that such processing could perturb platelet activation state. While our ultimate goal is to use completely untreated whole blood, the addition of the anticoagulant citrate was deemed a necessary stepping stone to this goal: its use allows direct comparison of results to “gold-standard” aggregometry methods that utilize anticoagulated blood (Harrison 2009). Furthermore, although citrate inhibits the coagulation cascade, it does not influence initial interactions of platelets with VWF surfaces, making our technique nominally independent of the use of this particular anticoagulant; future studies with non-anticoagulated blood are planned to verify this.

The citrate-treated whole blood samples were compared to citrate-treated whole blood to which the integrin-blocking c7E3-Fab fragment ReoPro was added. Commonly used in clinical settings to inhibit platelet-platelet aggregation and thrombus build-up, ReoPro alters platelet function in a manner that directly impacts surface interactions, a very useful parameter to manipulate for the characterization of the flow device and for assessing its possible assay applications.

3.1 Device design and dimensional characterization

A detailed understanding of the physics governing fluid flow between parallel plates led to a device design that provides controlled shear rates, minimizes edge effects, and significantly reduces blood sample volumetric flow rate

relative to commercial systems. Key design features include the comparatively small height-to-width chamber aspect ratio (1:40), a central interaction field of view far from any edge effects, and a comparatively thin blood layer thickness (50 μm) that results in a very low total blood volume (3.5 μL) contained by the device. Platelets can undergo a broad range of shear rates inside blood vessels, from low venous shear rates (50–200 s^{-1}) to pathophysiological shear rates in stenosed arteries (40,000 s^{-1}) (De Groot and Sixma Jan 2007). The highest shear rates in normal circulation range from 500 to 5,000 s^{-1} , and VWF-mediated platelet adhesion to a damaged vessel wall occurs at shear rates above a threshold of 500–800 s^{-1} . While this work focuses on studying platelet-VWF specific interactions at 1,500 s^{-1} , a shear rate generally found within the arteriole flow and in small arteries, future work will examine additional shear rates as specific disease states and physiological scenarios are studied. Fluid dynamic calculations show that the general performance characteristics of our parallel-plate flow device (in particular, absence of significant edge effects) apply over a broad range of shear rates from “venous” (50–200 s^{-1}) to arterial (large and small, 300 s^{-1} –1,500 s^{-1}) and “capillary” (2,000 s^{-1}) (De Groot and Sixma Jan 2007).

Realizing reproducible devices requires reproducible dimensional control, necessitating detailed characterization of multiple completed devices. Figure 5 shows that the white-light interferometrically-measured dimensions of the laser-patterned, coverslip-bonded PSA layer, which defines the boundaries of the parallel-plate flow chamber, agree favourably with the design.

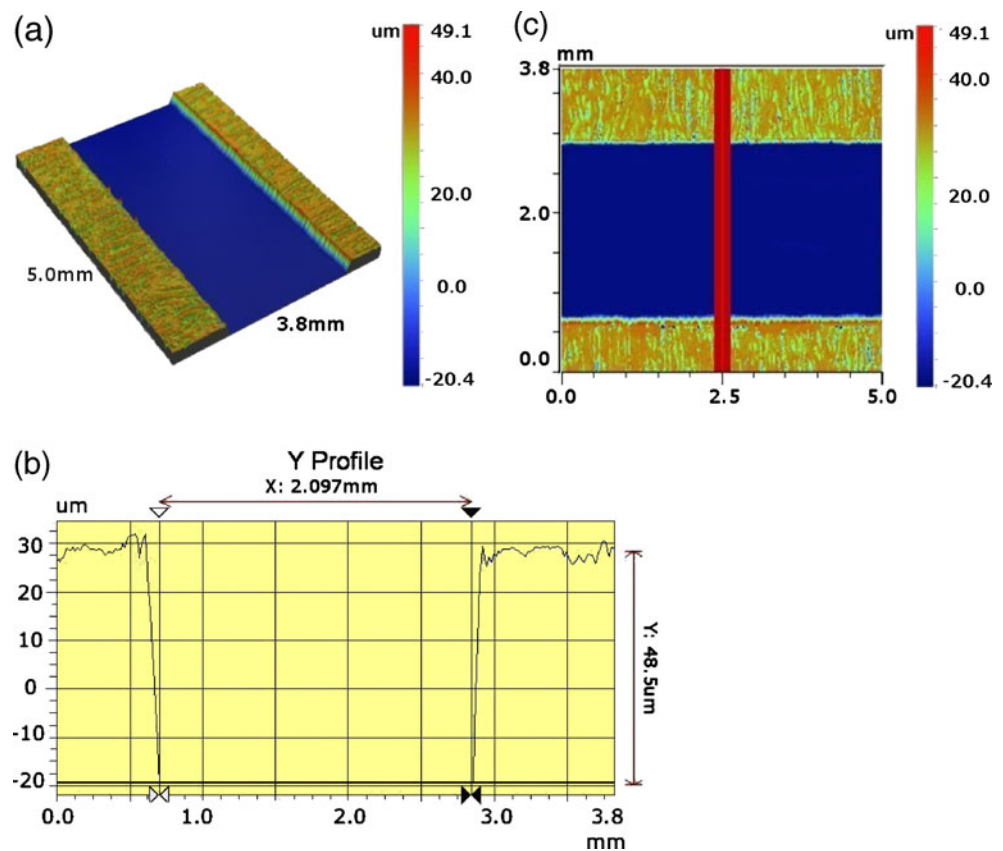
The height of the PSA measures 48.5 μm (material thickness specification: 50 μm), while the overall width of the flow path, 2.10 mm, is within 5% of the 2.0 mm design target. The sidewall roughness associated with the manufacturing process and adhesive ingress into the channel were measured using brightfield microscopy; the maximum ingress was 35 μm from a series of ten measurements, five of them along each channel sidewall. This PSA ingress is insignificant to the operation of the device due to the geometry and very low aspect ratio (1:40) of the flow path. The measured dimensions for flow path height and width, compared to the design dimensions, imply a difference of wall shear force of just over 1% relative to design at the initial target flow rate.

3.2 Protein layer deposition and characterization

3.2.1 Ellipsometric thickness and uniformity determination

Deposition of VWF on oxide-coated Si wafer pieces was accomplished as described in the Section 2. Ellipsometry was used to characterise the homogeneity of protein layer

Fig. 5 Dimensional characterization of fabricated microfluidic parallel-plate device using white-light interferometry. **(a)** 3-D view of a section of the device, highlighting the relative smoothness of the glass substrate (Ra 42 nm) and the surface topology of the adhesive film (Ra 4.75 μm). **(b)** Dimensional measurements taken along the cross section of the device indicated by the red band in part **(c)**. Measured dimensions are within a few percent of the original design parameters for the device. (Ra is the arithmetic average of the absolute values of measured peak heights over the sampled region)



thickness (more precisely, the product of layer thickness \times density, as measured by the index of refraction) at multiple points on a given sample, and to assess sample-to-sample thickness variability.

Figure 6 shows the results of ellipsometric thickness measurement of VWF layers prepared from a range of solution-phase concentrations, all samples having the same incubation time, after rinsing and drying. The results show characteristics typical of an adsorption isotherm associated with monolayer formation (Almalah et al. 1995): increasing the protein solution concentration results in a thicker protein film for a constant adsorption time, until a saturation coverage is reached, at which point coverage plateaus. The curve has a larger slope at low protein solution concentrations when surface coverage is comparatively low, reaching a plateau in the high-concentration range of about 3 nm thickness, indicating the formation of a “protein monolayer”: increases in solution concentration do not cause increases in surface coverage in this regime because all available surface adsorption sites have filled.

In solution, individual VWF colloids have diameters from 60 to 200 nm (Slayter et al. 1985), while our measurements using dual-polarized interferometry reveal that the thickness of the protein monolayer on an oxidized silicon surface is \sim 19 nm when wet (in contact with PBS). Thus, ellipsometry shows that dehydration of the protein

layer diminishes its optically-measured thickness more than 6-fold.

The reproducibility of the VWF coating was evaluated by measuring two or more sets of samples (the standard deviations of which are represented by the error bars in Fig. 6(a)); for samples made with VWF solutions of 100 $\mu\text{g}/\text{mL}$ and higher concentrations, only a 3% variation in the ellipsometric thickness among multiple pairs of samples was observed. For coatings made from VWF solution concentrations from 10 to 70 $\mu\text{g}/\text{mL}$, the average variation of the thickness for multiple pairs of samples was approximately 16%. This difference in variance is directly attributable to the shape of the adsorption curve: where the surface coverage changes steeply with VWF solution concentration, adsorption time, or even sample purity will cause a comparatively larger difference in coverage. In contrast, near or in the plateau region of the adsorption curve, small changes in any of these parameters have a comparatively small effect on protein surface coverage. In combination with the high cost of purified VWF, this led us to choose an adsorption concentration barely onto the plateau of the curve, and the resultant 3% variance is quite acceptable for assay or biological research purposes.

To investigate the homogeneity of surface coverage over large sample areas, nine points were measured over an area

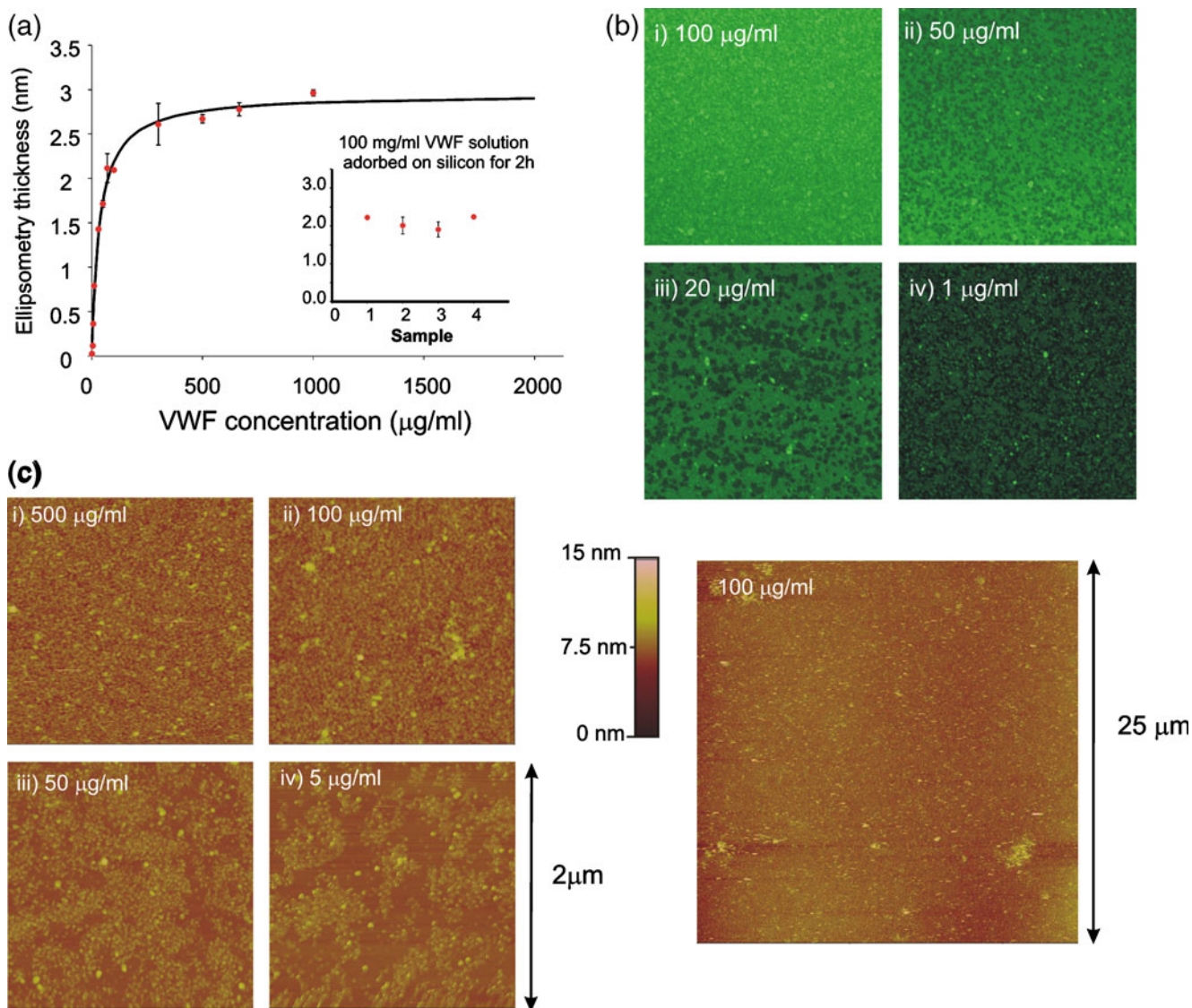


Fig. 6 (a) Ellipsometric characterization of VWF protein layers adsorbed on SiO_2 -covered Si wafers as a function of VWF concentration in aqueous PBS for an adsorption time of 2 h at 24°C . Inset: ellipsometrically measured thickness of four identically prepared samples (100 $\mu\text{g/ml}$ VWF solution, 2 hr adsorption); values are averages of nine measurement points on each sample over an area of 1 cm^2 . (b) $36.6 \times 36.6 \mu\text{m}^2$ fluorescence microscopy images of glass substrates on which VWF was absorbed from 100 (i), 50 (ii), 20 (iii)

and 1 (iv) $\mu\text{g/ml}$ VWF solutions for 2 h, followed by incubation with fluorescein isothiocyanate-labeled anti-VWF antibody. (c) At left: AFM height images over $2 \times 2 \mu\text{m}^2$ areas of VWF protein layers on SiO_2 -on-Si wafers for 2-hr adsorption from aqueous VWF solutions: 500 (i), 100 (ii), 50 (iii) and 5 (iv) $\mu\text{g/ml}$. At right: $25 \times 25 \mu\text{m}^2$ AFM height image of VWF adsorbed on Si/ SiO_2 from a 100 $\mu\text{g/ml}$ solution. Note: 3D versions of the images in part c) are presented as Supplementary Information

of 1 cm^2 for samples prepared with 100 $\mu\text{g/ml}$ VWF. The measurements show a maximum variation of dry VWF thickness for a single sample of 10%, confirming the homogeneity of the coating across a relatively large sample area (five times the area defined by the flow path in our parallel plate flow device).

An additional study was conducted to determine the influence of incubation time on the protein layer thickness. Two sets of samples, one made with solutions of VWF at concentrations of 10 $\mu\text{g/ml}$ and another set made with solutions of 100 $\mu\text{g/ml}$, were incubated on silicon surfaces

for 1, 2, and 4 h. No significant difference was observed in the thickness of the protein layer for a given concentration over these time periods.

3.3 AFM: Coverage uniformity results

While atomic force microscopy is most often used to characterize surface morphology on the nanometer scale, we used AFM chiefly to characterize the uniformity of VWF surfaces. The protein was adsorbed onto oxidized Si wafer substrates from VWF solution concentrations (in

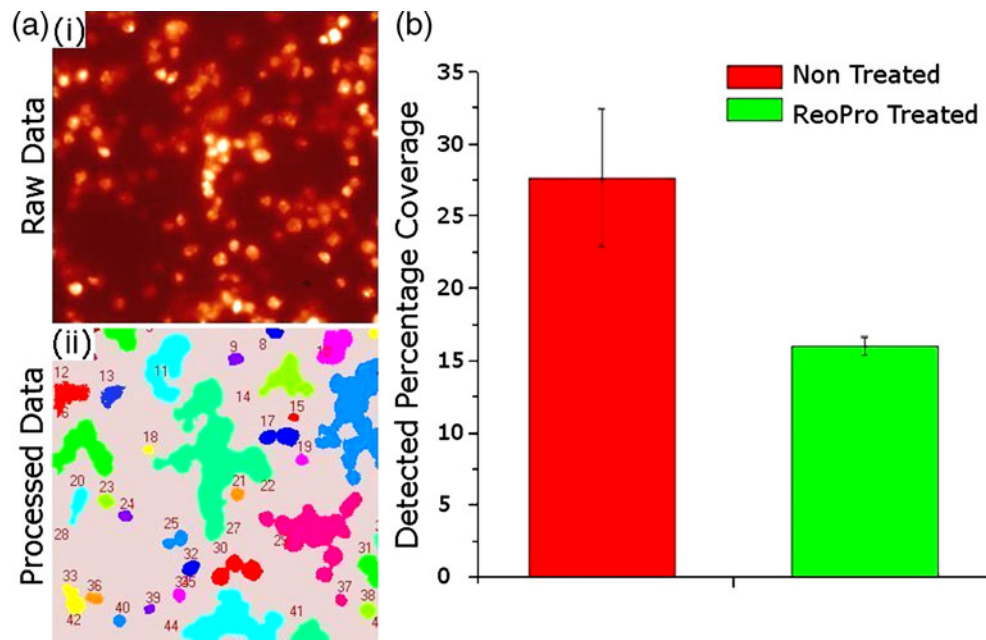


Fig. 7 Image acquisition and analysis for fluorescently labeled platelets adhering to the VWF-coated surface in the parallel-plate device. **(a)** (i) Raw image (single frame, $t=115$ s after starting blood flow at a wall shear stress of 6 N/m^2) taken directly from the CCD camera. Depth of focus ($20 \mu\text{m}$), frame rate (24 frames/sec), and fluid flow rate are such that only platelets adhering to the protein-coated glass surface appear as bright spots in the image; all other platelets are completely out of focus. (ii) Result of implementing the custom thresholding algorithm on the image in (i): each detected particle or

contiguous cluster is highlighted and assigned a color and unique number. **(b)** Compilation of results from image analysis data taken from ten individual flow runs: 5 untreated whole blood samples (red bar), 5 ReoPro (c7E3-Fab fragment)-treated samples (green bar). Percent surface coverage, calculated from data processed as shown in (a)(ii), reveals a clear distinction between untreated samples (28% coverage, red bar) and ReoPro-treated samples (16% coverage, green bar), showing that platelets are significantly “less sticky” for the latter samples

PBS) from 1 to $750 \mu\text{g/mL}$. Silicon substrates were chosen rather than glass coverslips in this case because they provide a much flatter surface on the nm scale; the roughness of the glass precluded either measurement of protein layer morphology or determination of coverage uniformity (Toscano and Santore 2006). Because the oxidized Si surface has very similar chemical composition to glass, our goal of determining coverage uniformity is best served by the use of this substrate.

Figure 6(c) shows $2 \mu\text{m}^2$ AFM images of samples prepared from 5, 50, 100, and $500 \mu\text{g/mL}$ VWF solutions (3D versions of the AFM images of these same samples are presented in the Supplementary Information as Figure S1). Only at low concentrations, i.e. 5 and $50 \mu\text{g/mL}$, does AFM show that the surface is not fully covered by protein; for concentrations of $100 \mu\text{g/mL}$ and higher, the surface is uniformly coated.

Figure 6(c) includes an image over an area of $625 \mu\text{m}^2$ of a sample prepared with a VWF solution of $100 \mu\text{g/mL}$. AFM images of 625 and $5,625 \mu\text{m}^2$ areas confirm that coverage is uniform over these larger areas.

To verify that observed morphology and coverage variations were not an artifact of the substrate, we imaged a blank, oxidized Si sample. Its AFM image was essentially

identical to the non-coated regions of the low-coverage VWF-coated samples, as typified, e.g., by significant portions of the $5 \mu\text{g/mL}$ image in Fig. 6(c).

3.3.1 Fluorescence characterization via antibody binding

To confirm the biochemical functionality and uniformity of VWF protein layers, surfaces prepared on bare glass substrates from solution concentrations ranging from 1 to $100 \mu\text{g/mL}$ were incubated with a fluorescently labeled anti-VWF antibody. The images in Fig. 6 show greater fluorescent emission in samples prepared with higher VWF concentration, indicating a higher amount of protein adsorbed on the surface.

Figure 6 also shows that samples prepared with VWF concentrations of $100 \mu\text{g/mL}$ form a continuous layer that uniformly covers the surface. These results, which are qualitatively consistent with those obtained by ellipsometry and AFM with regard to the amount and distribution of protein on the surface, confirm the functionality of the protein vis-à-vis binding to a specific antibody after surface immobilization.

As mentioned in the Section 2, VWF-coated surfaces were “blocked” using BSA prior to whole blood assay use.

Comparison of platelet surface coverage on VWF with and without BSA blocking and otherwise identical conditions, however, indicate that the blocking buffer does not affect the efficiency of platelet adhesion to any measurable extent. The blocking step is therefore only precautionary: in the seemingly unlikely event that any of the glass surface were to be left uncovered, BSA would prevent exposure of platelets to the glass surface, which would be likely to activate them.

Overall, the results from multiple characterization methods, as well as the lack of any significant difference in platelet adhesion due to BSA blocking, lead to the conclusion that adsorption of VWF on a glass (or glass-like) surface from a VWF solution of 100 $\mu\text{g}/\text{mL}$ or higher, for a duration of at least 2 h at room temperature, yields a uniform, well-packed monolayer of active protein without gaps in coverage that could artifactually activate platelets.

3.4 Whole blood assay: image analysis results

In total, ten whole-blood assay runs were performed over a period of two days using blood from multiple donors. Each donated blood sample was treated with citrate, divided, and assayed under both normal and ReoPro-treated conditions under which the platelet $\alpha\text{IIb}\beta_3$ receptors are significantly inhibited.

Figure 7(a)(i) shows raw data obtained from the optical microscope and CCD camera for fluorescent platelets bound to the VWF-coated glass coverslip surface of our platelet assay device. This image was obtained at $t=115$ s, frame no. 2,750 ($t=0$ s and frame no. 0 mark the initial time point of image capture), for an untreated blood sample from a healthy donor at an effective wall shear stress of 6 N/m^2 (corresponding to a typical arterial shear rate of 1,500 s^{-1}). This flow duration is long enough to provide readily measurable platelet coverages, but short enough that larger thrombi or “clumps”, which might impede the flow of blood and platelets over the imaging region and so affect the results, have not formed.

Figure 7(a)(ii) shows the results of image processing the data in (i) using our custom software: each separately-defined region is numbered and colored for visualisation, the colored regions representing the presence of one or more platelets and the pinkish-grey regions representing no detected platelets, i.e. locations where the fluorescence signal is below threshold. The software returns the number of pixels detected as a percentage of the overall number of pixels in the frame, giving a detected surface coverage of platelets per image, the value being 31.7% for this particular image.

Figure 7(b) shows the detected average surface coverage from 10 individual flow runs, five ReoPro-treated whole blood samples (green bar) and five untreated whole blood samples (red bar), in each case at 2,750 frames ($t=115$ s)

after the start of the flow run. Standard deviations, included on both coloured bars in the figure, confirm that the difference between untreated and treated blood is significant: surface coverage is approximately $16\pm 1\%$ in the case of ReoPro-treated blood and approximately $27\pm 5\%$ in the case of untreated blood ($P=0.002$). In essence, ReoPro treatment interferes with a key receptor involved in binding to VWF, rendering platelets “less sticky,” and this effect is readily quantified with our assay device.

This straightforward method of image analysis clearly reveals distinctions in platelet-surface interactions between normal and treated whole blood samples using our device, validating both the device design and the analysis method. The results illustrate as well how measurements of platelet surface coverage under conditions of controlled shear and reproducible surface functionalization have possible diagnostic relevance. Using this platform, Lincoln et al. (Lincoln et al. 2010) have shown how alternative, more sophisticated image analysis methodologies can be used to glean more information about the nature of platelet-surface interactions.

4 Summary and conclusions

We have developed a new parallel-plate flow chamber incorporating a number of advantages over existing commercial systems. The reduced chamber dimensions, particularly height, result in a significant (32x) reduction in required flow rate for a given shear force. The combination of materials and assembly technique eliminates the need for the specialized hardware used to seal commercial devices. This has the additional advantage of making a more user-friendly platform while enabling the preparation and assembly of a number of devices at once to increase throughput. Further, the design strategy and materials involved in device manufacture lend themselves well to both rapid prototyping and mass production techniques, pointing the way towards making this device a hugely cost-effective alternative to commercial systems.

We also demonstrated and documented a method to reproducibly immobilise a uniform protein coating on the region of interest within the custom device, a key to its successful operation. Using a combination of independent techniques, coating homogeneity and uniformity of coverage were characterized over a large area, sample-to-sample variations in coating uniformity were measured, protein surface morphology was recorded, and the biochemical functionality of the immobilized coating was determined.

As a means to characterize the efficacy of the device, we developed a custom software algorithm to rapidly quantify the percentage coverage of platelets at a given time point during whole-blood flow analysis, allowing quantitative

distinction of differences in surface coverage between normal and treated samples. While the analysis strategy is relatively simple and other, more sophisticated techniques have been recently developed (Lincoln et al. 2010), it illustrates the functional properties of the device in a meaningful fashion that may lead to diagnostic applications.

Overall, the system described here represents a major first step towards a medical research system that can screen large numbers of clinical samples at acceptable cost without the need for extensive operator training, leading to the determination of relationships between platelet activation state, platelet function, and states of health and disease. Ultimately, we believe that the results from such studies, in combination with a mass-produced version of the device described in this paper, will enable a clinically important point-of-care diagnostic device.

Acknowledgements The authors gratefully acknowledge the help of Dr. Cedric Volcke with the AFM measurements, and related discussions, and the help of Dr. Helen Berney and Dr. Arun Harish, Field Applications Scientist, Fairfield Group Ltd., UK with the dual-polarized interferometry and related discussions. This material is based upon works supported by the Science Foundation Ireland under Grant No. 05/CE3/B754.

References

- C.H. Ahn, J.W. Choi, G. Beaucage, J.H. Nevin, J.B. Lee, A. Puntambekar, J.Y. Lee, Disposable Smart lab on a chip for point-of-care clinical diagnostics. *Proc IEEE* **92**, 154–173 (2004)
- K. Almalah, J. McGuire, R. Sproull, A Macroscopic Model for the Single-Component Protein Adsorption-Isotherm. *J Colloid Interface Sci* **170**, 261–268 (1995)
- H. Becker, L.E. Locascio, Polymer microfluidic devices. *Talanta* **56**, 267–287 (2002)
- T. Boone, Z.H. Fan, H. Hooper, A.J. Ricco, H.D. Tan, S. Williams, Plastic advances microfluidic devices. *Anal Chem* **74**, 78A–86A (2002)
- D.C. Brown, R.S. Larson, Improvements to parallel plate flow chambers to reduce reagent and cellular requirements. *BMC Immunol* **2**, 1–7 (2001)
- H. Bruus, *Theoretical Microfluidics* (Oxford University Press, Oxford, 2007)
- W.C. Chang, L.P. Lee, D. Liepmann, Biomimetic technique for adhesion-based collection and separation of cells in a microfluidic channel. *Lab Chip* **5**, 64–73 (2005)
- R. Daw, J. Finkelstein, Lab on a chip. *Nature* **442**, 367–367 (2006)
- P.G. De Groot, J. Sixma Jan, Perfusion Chambers, Chapter 32, in *Platelets*, ed. by A.D. Michelson, 2nd edn. (Elsevier/Academic Press, San Diego, 2007), pp. 575–585
- J. El-Ali, P.K. Sorger, K.F. Jensen, Cells on chips. *Nature* **442**, 403–411 (2006)
- H. Elwing, Protein absorption and ellipsometry in biomaterial research. *Biomaterials* **19**, 397–406 (1998)
- C. Fillafer, G. Ratzinger, J. Neumann, Z. Guttenberg, S. Dissauer, I. Lichtscheidl, M. Wirth, F. Gabor, M. Schneider, An acoustically driven biochip—impact of flow on the cell-association of targeted drug carriers. *Lab Chip* **9**(19), 2782–2788 (2009)
- J. Garcia-Cordero, A.J. Ricco, *Lab on a Chip (General Philosophy) in Encyclopedia of Micro- and Nanofluidics*, 962–969 (Springer, Berlin, 2008)
- E. Gutierrez, B. Petrich, S. Shattil, M. Ginsberg, A. Groisman, A. Kasirer-Friede, Microfluidic devices for studies of shear dependent platelet adhesion. *Lab Chip* **8**, 1486–1495 (2008)
- P. Harrison, Platelet function analysis. *Blood Rev* **19**, 111–123 (2005)
- P. Harrison, Assessment of platelet function in the laboratory. *Hamostaseologie* **29**, 25–31 (2009)
- A.S. Kantak, B.K. Gale, Y. Lvov, S.A. Jones, Platelet function analyzer: Shear activation of platelets in microchannels. *Biomed Microdevices* **5**, 207–215 (2003)
- M.H. Kroll, J.D. Hellums, L.V. McIntire, A.I. Schafer, J.L. Moake, Platelets and shear stress. *Blood* **88**, 1525–1541 (1996)
- B. Lincoln, A.J. Ricco, N.J. Kent, L. Basabe-Desmots, L.P. Lee, B. D. MacCraith, D. Kenny, G. Meade, Integrated system for the study of fluid shear-mediated platelet interactions with Von Willebrand Factor protein surfaces using microliter volumes of whole blood. doi:10.1016/j.ab.2010.05.030
- H. Lu, L.Y. Koo, W.C.M. Wang, D.A. Lauffenburger, L.G. Griffith, K. F. Jensen, Microfluidic shear devices for quantitative analysis of cell adhesion. *Anal Chem* **76**, 5257–5264 (2004)
- A.D. Michelson, *Platelets 2nd Ed* (Academic Press, USA, 2006), pp. 145–158
- N.A. Mody, O. Lomakin, T.A. Doggett, T.G. Diacovo, M.R. King, Mechanics of transient platelet adhesion to von Willebrand factor under flow. *Biophys J* **88**, 1432–1443 (2005)
- K. Nakanishi, T. Sakiyama, K. Imamura, On the adsorption of proteins on solid surfaces, a common but very complicated phenomenon. *J Biosci Bioeng* **91**, 233–244 (2001)
- NI Vision Concepts Manual. Ed. Corporation, N.I. (2000–2005). <http://www.ni.com/pdf/manuals/372916e.pdf>
- N. Saeidi, E. Sander, J. Ruberti, Dynamic shear-influenced collagen self-assembly. *Biomaterials* **30**(34), 6581–6592 (2009)
- U. Schaff, M. Xing, K. Lin, N. Pan, N. Jeon, S. Simon, Vascular mimetics based on microfluidics for imaging the leukocyte—endothelial inflammatory response. *Lab Chip* **7**(4), 448–456 (2007)
- B. Schmidt, P. Huang, K. Breuer, M. Lawrence, Catch strip assay for the relative assessment of two-dimensional protein association kinetics. *Anal Chem* **80**(4), 944–950 (2008)
- H. Slayter, J. Loscalzo, P. Bockenstedt, R.I. Handin, Native Conformation of Human Vonwillebrand Protein— Analysis by Electron-Microscopy and Quasi-Elastic Light-Scattering. *J Biol Chem* **260**, 8559–8563 (1985)
- S.H. Tam, P.M. Sassoli, R.E. Jordan, M.T. Nakada, Abciximab (ReoPro, chimeric 7E3 Fab) demonstrates equivalent affinity and functional blockade of glycoprotein IIb/IIIa and alpha(v) beta(3) integrins. *Circulation* **98**, 1085–1091 (1998)
- P. Tengvall, I. Lundstrom, B. Liedberg, Protein adsorption studies on model organic surfaces: an ellipsometric and infrared spectroscopic approach. *Biomaterials* **19**, 407–422 (1998a)
- P. Tengvall, A. Askendal, I. Lundstrom, Studies on protein adsorption and activation of complement on hydrated aluminium surfaces *in vitro*. *Biomaterials* **19**, 935–940 (1998b)
- W. Thomas, Catch bonds in adhesion. *Annu Rev Biomed Eng* **10**, 39–57 (2008)
- A. Toscano, M.M. Santore, Fibrinogen adsorption on three silica-based surfaces: Conformation and kinetics. *Langmuir* **22**, 2588–2597 (2006)
- G.M. Whitesides, E. Ostuni, S. Takayama, X.Y. Jiang, D.E. Ingber, Soft lithography in biology and biochemistry. *Annu Rev Biomed Eng* **3**, 335–373 (2001)
- P. Yager, G.J. Domingo, J. Gerdes, Point-of-care diagnostics for global health. *Annu Rev Biomed Eng* **10**, 107–144 (2008)

- J.J. Zwaginga, G. Nash, M.R. King, J.W. Heemskerk, M. Frojmovic, M.F. Hoylaerts, K.S. Sakariassen, Flow-based assays for global assessment of hemostasis. Part 1: Biorheologic considerations. *J Thromb Haemost* **4**, 2486–7 (2006a)
- J.J. Zwaginga, K.S. Sakariassen, G. Nash, M.R. King, J.W. Heemskerk, M. Frojmovic, M.F. Hoylaerts, Flow-based assays for global assessment of hemostasis. Part 2: current methods and considerations for the future. *J Thromb Haemost* **4**, 2716–7 (2006b)
- J.J. Zwaginga, K.S. Sakariassen, M.R. King, T.G. Diacovo, E.F. Grabowski, G. Nash, M. Hoylaerts, J.W. Heemskerk, Can blood flow assays help to identify clinically relevant differences in von Willebrand factor functionality in von Willebrand disease types 1–3? *J Thromb Haemost* **5**, 2547–2549 (2007)